energies

MDPI

Article

Modeling and Performance Assessment of a NeWater System Based on Direct Evaporation and Refrigeration Cycle

Yilin Huo [1], Eric Hu [1,*] and Jay Wang [2]

[1] School of Electrical and Mechanical Engineering, Adelaide University, Adelaide, SA 5005, Australia; yilin.huo@adelaide.edu.au
[2] School of Engineering, Computer and Mathematical Sciences, Auckland University of Technology, Auckland 1010, New Zealand; jay.wang@aut.ac.nz
* Correspondence: eric.hu@adelaide.edu.au

Abstract

At present, the global shortage of water resources has led to serious challenges, and traditional water production technologies such as seawater desalination and atmospheric water harvesting have certain limitations due to inflexible operation and environmental conditions. This study proposes a novel water production system (called "NeWater" system in this paper), which combines saline water desalination with atmospheric water-harvesting technologies to simultaneously produce freshwater from brackish water or seawater and ambient air. To evaluate its performance, an integrated thermodynamic and mathematical model of the system was developed and validated. The NeWater system consists of a vapor compression refrigeration unit (VRU), a direct evaporation unit (DEU), up to four heat exchangers, some valves, and auxiliary components. The system can be applied to areas and scenarios where traditional desalination technologies, like reverse osmosis and thermal-based desalination, are not feasible. By switching between different operating modes, the system can adapt to varying environmental humidity and temperature conditions to maximize its freshwater productivity. Based on the principles of mass and energy conservation, a performance simulation model of the NeWater system was developed, with which the impacts of some key design and operation parameters on system performance were studied in this paper. The results show that the performances of the VRU and DEU had a significant influence on system performance in terms of freshwater production and specific energy consumption. Under optimal conditions, the total freshwater yield could be increased by up to 1.9 times, while the specific energy consumption was reduced by up to 48%. The proposed system provides a sustainable and scalable water production solution for water-scarce regions. Optimization of the NeWater system and the selection of VRUs are beyond the scope of this paper and will be the focus of future research.

Keywords: desalination; atmospheric water harvesting; condensation; heat and mass transfer; cooling tower

Academic Editors: Yiming Zhao and Haotian Ye

Received: 26 November 2025
Revised: 8 January 2026
Accepted: 15 January 2026
Published: 17 January 2026

1. Introduction

Water scarcity is one of the escalating global challenges today. According to data from the United Nations, more than 2 billion people are living in countries with high water stress [1,2]. At the same time, constantly changing climate patterns, rapid urbanization, and unsustainable water resource management practices have led to a reduction in available water resources, exacerbating freshwater shortages [3–5]. This issue puts pressure on social

production and people's lives in many regions, especially in arid and semi-arid areas, where relying solely on traditional water sources cannot meet current or future water supply demands [6]. This has created an urgent need for innovation in technologies for water production and recycling [7]. In order to solve this problem, many researchers have studied the development and evaluation of innovative technologies to address the global water crisis, and two main approaches have emerged: seawater desalination and atmospheric water harvesting [8,9].

Seawater desalination mainly uses reverse osmosis (RO) and thermal distillation such as membrane distillation (MD) [10,11]. RO is commercialized and widely applied because of its cost-effectiveness. RO also allows for different membrane designs and structures, and it can reach a salt retention rate of up to 90% [12–14]. However, the drawbacks of RO technology include the need for strict pretreatments, the inability to stop easily during operation without the risk of damaging membrane components, and its limited ability to remove genetic pollutants that may exist in raw water. The RO system needs to operate under high pressure to overcome osmotic pressure [15]. Also, Shin, Koo, and Lee [16] noted that membrane pollution and scaling reduce operational stability and increase maintenance requirements [16]. At the same time, RO requires a relatively complex pretreatment process before operation, and once the operation is started, it is difficult to stop it halfway, as this can easily cause damage to membrane components. In addition, RO membranes cannot effectively remove genetic pollutants that may exist in raw water. The above factors lead to complex system operations and high investment demands, making it difficult to promote RO technology in underdeveloped areas and remote rural areas [17]. Additionally, transporting seawater to inland areas would also introduce additional logistics and operational burdens [18].

As another efficient seawater desalination method, MD has attracted great academic interest due to its very good recovery rate and lower energy usage [19]. However, MD also has limitations, including its dependence on high-temperature heat sources or nearby waste heat, relatively low membrane flux, and sensitivity to operating conditions. Lu et al. [20] found that MD can effectively produce freshwater when a high-temperature heat source is available. However, MD generally requires substantial supplies of steam or waste heat and relies on specific operating conditions. Traditional MD membranes also have low water flux, which limits their efficiency. To address this issue, Gong et al. [21] made a new membrane that blocks almost all NaCl and microbes, which allows for very fast desalination. This method still depends on making high-temperature, high-flux membranes. This limits large-scale use; MD is mainly used for small-scale operations or to reduce concentrate production [22].

Apart from seawater desalination, atmospheric water harvesting has become an effective means of decentralized water production, overcoming the challenges of long-distance transport or delivery of drinking water in rural areas [23]. Atmospheric water harvesting technologies can be classified according to their working principles into condensation methods, sorption-based atmospheric water harvesting (SAWH), and other methods [24]. Condensation methods like passive radiative condensers reduce the air temperature below the dew point to condense water vapor in the air into liquid water [25]. This method does not require any additional energy input but is highly dependent on weather conditions such as RH, sky emissivity, and air velocity, and the water yield is low [26].

SAWH is one of the main methods of atmospheric water harvesting [27]. This method uses sorbents or absorbent materials to adsorb and capture water from the air and release the water [28]. It has the advantages of being able to collect and obtain water under low relative humidity values and can be integrated with other technologies [29]. Ying et al. [30] designed a continuous SAWH system using different characteristic sorbents and tested

its energy efficiency, showing that their solar-powered continuous SAWH system could operate effectively year-round in nearly 40% of global areas. However, environmental temperature and operating humidity had significant impacts on the system's performance, posing higher requirements for sorbent selection.

The above review shows that there are still multiple limitations in current water production research. Although seawater desalination is mature, its high energy demand and limited applicability restrict its use in water-scarce regions [31,32]. Atmospheric water harvesting has potential, but environmental sensitivity and low technological maturity limit its practical deployment [33]. These research deficiencies together indicate that current water production technologies struggle to simultaneously meet the requirements of strong adaptability, low energy consumption, flexible operation, and wide regional applicability [34].

To develop a freshwater desalination or production system for areas or scenarios where traditional RO and thermal-based technologies are not feasible, a NeWater system integrated based on a direct evaporation unit and a refrigeration cycle device is proposed in this paper. This study is motivated by the need for adaptable hybrid systems that can produce freshwater from both saline water and atmospheric humidity. The aim of this research is to reveal the relationships between the operating parameters of the NeWater system and its design parameters, and the overall system performance. This study focuses on modeling solutions for the heat and mass transfer processes in the NeWater system, especially for the direct evaporation unit, and establishes a calculation framework suitable for the NeWater system. This study not only promotes the development of direct evaporation unit modeling methods in theory but also provides a sustainable water production solution with engineering feasibility and scalability for water-scarce regions.

2. The NeWater System

2.1. System Description

The proposed NeWater system uses green electrical power to drive its processes for desalinating saline water and harvesting water from ambient air. Unlike RO systems, the NeWater system can be operated intermittently. It can operate in three modes: opened loop (OL), closed loop (CL), and combined or hybrid loop (CHL). The detailed configuration and valve control logic for each mode are described in the following section. The schematic of the NeWater system is shown in Figure 1. The system is composed of valves, a vapor compression refrigeration unit (VRU), which includes a compressor, an expansion valve, an evaporator heat exchanger (EHE), a condenser heat exchanger (CHE), a cooling recovery heat exchanger (HE1), an ambient air heat exchanger (HE2), and a direct evaporation unit (DEU), i.e., cooling tower, water tanks, and a fan.

2.2. Structure and Operation Modes of the NeWater System

The system operation mode can be flexibly adjusted to the OL, CL, or CHL modes by controlling the three valves (Val_1, Val_2, and Val_3).

When valves Val_1 and Val_3 are fully opened and valve Val_2 is closed, the system operates in the OL mode, allowing 100% ambient air to circulate through the system. When valve Val_2 is fully opened, while valves Val_1 and Val_3 are closed, the system operates in the CL mode, where the air is fully recirculated within the system, i.e., no ambient air intake. When all three valves (Val_1, Val_2, and Val_3) are partially opened, the system operates in the CHL mode, allowing intake of some ambient air and recycling of part of the air.

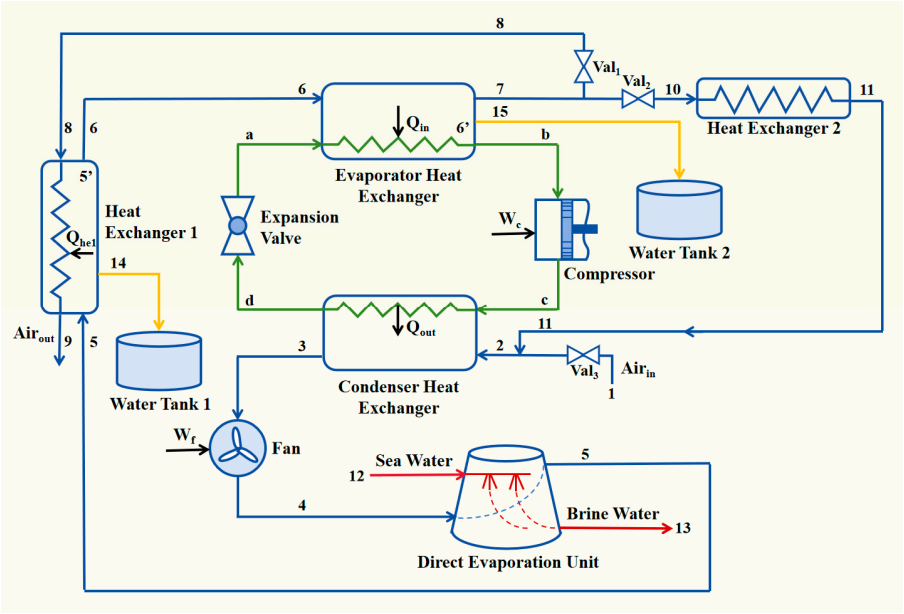

Figure 1. Schematic diagram of NeWater system.

In the CHL mode, ambient air with the properties (T_1, $\dot{m}_{a1}$, RH_1) enters the system through the semi-opened valve Val_3 and meets recycled air from point 11 with properties (T_{11}, $\dot{m}_{a11}$, RH_{11}). The mixed stream at state 2 (T_2, $\dot{m}_{a2}$, RH_2) travels to the condenser heat exchanger (CHE), where it is heated by the condensing heat (Q_{out}) of the refrigeration unit. After leaving the CHE at state 3 (T_3, $\dot{m}_{a3}$, RH_3), the air stream is further heated by the fan, its state turns to state 4 (T_4, $\dot{m}_{a4}$, RH_4), and it continues to the inlet of the DEU.

Inside the DEU, the air is in direct contact with saline water (T_{w12}, $\dot{m}_{w12}$) entering from water inlet 12. The water and the air flows leave the DEU as brine at state 13 (T_{w13}, $\dot{m}_{w13}$) and as humid air near saturation at state 5 (T_5, $\dot{m}_{a5}$, RH_5), respectively. The brine at state 13 is discharged from the system, and the associated sensible heat loss is accounted for in the overall energy balance of the DEU.

The humid air at state 5 then passes through HE1 to be precooled by exhaust air 8 from valve Val_1, before entering the evaporator heat exchanger (EHE) at state 6 (T_6, $\dot{m}_{a6}$, RH_6). There may be some liquid water condensed in HE1. The condensed water generated in this process is collected in water tank 1 at state 14 (T_{w14}, $\dot{m}_{w14}$).

In the EHE, the air loses heat (Q_{in}) to the evaporator and its temperature is reduced. During this process (6 $\rightarrow$ 7 and 15), freshwater can be produced and collected in the water tank 2 at state 15 (T_{w15}, $\dot{m}_{w15}$).

After losing moisture, the air leaves the EHE at a relatively low temperature, T_7, and is divided into two streams: some air is released via valve Val_1 after passing through HE1; the rest is recirculated, after HE2, to meet the ambient air intake 1. In HE2, the air is warmed up by the ambient environment from state 10 to state 11.

3. Mathematical Modeling of NeWater System

The mathematical simulation model of the NeWater system is established to quantitatively describe the heat and mass transfer processes among the air, water, and refrigerant within the system at a steady state.

3.1. Model Assumptions

To simplify the model and make it more suitable for engineering calculations, several reasonable assumptions made in the model are as follows:

1. The system operates under steady-state conditions;
2. The apparatus and the cooling water recirculation loop are thermally insulated from the surroundings;
3. Heat transfer by radiation is neglected;
4. Water loss caused by drift is considered negligible;
5. Air and water are uniformly distributed at the inlets, and this uniform distribution is maintained throughout the process;
6. The outlet air from the direct evaporation unit is assumed to have a constant relative humidity;
7. When air passes through HE1 and HE2, its outlet temperature is predefined by the system conditions.

While these assumptions simplify the analysis, they are recognized as sources of uncertainty. In addition, this is a steady-state model, which is incapable of revealing and simulating the dynamic performance of the system when input parameters change.

3.2. Process-Based Mathematical Models

In the NeWater system, several fluids interact through heat and mass transfer in different modules. Each process between two or more thermodynamic states represents a distinct exchange of energy and mass, including mixing, cooling, condensation, and evaporation.

Modeling these processes is essential for predicting outlet conditions and evaporation and condensation rates, and evaluating the overall energy balance of the system. The following subsections describe the mathematical models for each fluid process in detail.

Process 1 and 11 → 2 (air mixing): The ambient air that enters through valve Val_3 from point 1 mixes with the circulating air from point 11 and flows to point 2. The total mass of dry air and water vapor is conserved during mixing. The humidity ratio and enthalpy of the mixed air are determined by the mass flow rates and thermodynamic properties of the two inlet air streams. The mass and energy balances for this process are expressed by the following governing equations, which allow for the calculation of the outlet humidity ratio and enthalpy based on the inlet conditions and governing thermodynamic relationships; all mathematical symbols used are defined in the Nomenclature Section following the main text [35]:

$$\dot{m}_{a2} + \dot{m}_{v2} = \dot{m}_{a1} + \dot{m}_{v1} + \dot{m}_{a11} + \dot{m}_{v11} \quad (1)$$

$$\dot{m}_{a1}h_{a1} + \dot{m}_{v1}h_{v1} + \dot{m}_{a11}h_{a11} + \dot{m}_{v11}h_{v11} = \dot{m}_{a2}h_{a2} + \dot{m}_{v2}h_{v2} \quad (2)$$

Processes 2 → 3 and c → d (heat exchange in CHE): The air is heated by the condensing heat from the refrigeration unit in the CHE, and the outlet air reaches state 3. The total mass of dry air and water vapor is conserved during heat exchange. The mass and energy balances for this process are expressed by the following governing equations [36]:

$$\dot{m}_{a2} + \dot{m}_{v2} = \dot{m}_{a3} + \dot{m}_{v3} \quad (3)$$

$$\dot{Q}_{out} + \dot{m}_{a2}h_{a2} + \dot{m}_{v2}h_{v2} = \dot{m}_{a3}h_{a3} + \dot{m}_{v3}h_{v3} \quad (4)$$

$$\dot{Q}_{out} = (COP + 1) \times \dot{W}_c \quad (5)$$

Process 3 → 4 (passing fan): The heated air from the condenser exchanger is sucked into and driven by the fan, which provides power W_f. The air passes through the fan without any heat exchange with the surroundings. The total mass of dry air and water vapor is conserved during this process. The humidity ratio and enthalpy of the air remain

determined by the inlet conditions and the fan operation. No condensation or evaporation occurs in this process:

$$\dot{m}_{a3} + \dot{m}_{v3} = \dot{m}_{a4} + \dot{m}_{v4} \tag{6}$$

$$\dot{W}_f + \dot{m}_{a3}h_{a3} + \dot{m}_{v3}h_{v3} = \dot{m}_{a4}h_{a4} + \dot{m}_{v4}h_{v4} \tag{7}$$

Processes 4 → 5 and 12 → 13 (air–water meeting in DEU): The air at state 4 enters the DEU and meets the seawater entering at inlet 12. The air and water flow counter to each other and are in direct contact. The air becomes humid and approaches saturation at state 5, while the water becomes concentrated brine at state 13. The total mass of dry air and water vapor is conserved, while evaporation occurs from the water to the air. The humidity ratio and enthalpy of the air and water streams are determined by the mass flow rates and thermodynamic properties of the two inlet streams.

The energy and mass balances are expressed through the following equations, which account for both the heat transferred between air and water and the evaporation occurring in the DEU, in combination with the governing thermodynamic relationships [35]:

$$\dot{m}_{a4} + \dot{m}_{v4} + \dot{m}_{w12} = \dot{m}_{a5} + \dot{m}_{v5} + \dot{m}_{w13} \tag{8}$$

$$\dot{m}_{w12}h_{w12} + \dot{m}_{a4}h_{a4} + \dot{m}_{v4}h_{v4} = \dot{m}_{w13}h_{w13} + \dot{m}_{a5}h_{a5} + \dot{m}_{v5}h_{v5} \tag{9}$$

The Merkel number is used to quantify the effectiveness of heat and mass transfer. The evaporation rate is calculated based on the Merkel number and the difference in humidity ratio between the water surface and the air using the method described in [37,38]. The process:

$$Merkel\ Number = \frac{Ah_m}{\dot{m}_{w12}} \tag{10}$$

$$\text{Merkel Number} = 1.5655 \times \left(\frac{\dot{m}_{w12}}{\dot{m}_{a3}}\right)^{-0.672} \tag{11}$$

$$\dot{m}_{evap} = Ah_m\left(\omega^* - \frac{\omega_4 + \omega_5}{2}\right) \tag{12}$$

$$\omega^* = 0.622\frac{0.611 \times \exp\left(\frac{8.635 \times (T_{w12}+T_{w13})}{0.5 \times (T_{w12}+T_{w13})+237.3}\right)}{101,300 - 0.611 \times \exp\left(\frac{8.635 \times (T_{w12}+T_{w13})}{0.5 \times (T_{w12}+T_{w13})+237.3}\right)} \tag{13}$$

where ω^* (kg/kg) is the humidity ratio of saturated air at the water surface temperature, representing the equilibrium moisture content at the interface between the air and the cooling water.

Processes 5 → 6 and 14, and 8 → 9 (passing HE1): Humid air from state 5 passes through HE1, where it is precooled before entering the evaporator heat exchanger at state 6. This process aims to recover part of the cooling capacity from the exhaust air, thereby improving system efficiency.

The air may experience either sensible cooling only or a combination of sensible cooling and condensation, depending on whether the outlet state reaches saturation. The outlet temperature is preliminarily determined based on the valve control parameter, after which the vapor pressure and relative humidity are evaluated. In this process, we assume the following:

$$T_6 = T_5 - 2 \times OP_{val1}, \tag{14}$$

and check whether condensation occurs during the process by the following equations:

$$p_{v5} = RH_5 \times \exp\left(\frac{17.27 \times T_5}{T_5 + 237.3}\right), \tag{15}$$

We calculate RH_6 by assuming $p_{v5} = p_{v6}$:

$$RH_6 = \frac{RH_5 \times \exp\left(\frac{17.27 \times T_5}{T_5 + 237.3}\right)}{\exp\left(\frac{17.27 \times T_6}{T_6 + 237.3}\right)} \tag{16}$$

When the relative humidity at the outlet (RH_6) remains below 100%, the process involves only sensible cooling. Otherwise, condensation occurs, and both latent and sensible heat transfer are considered in the energy balance. Accordingly, the mass and energy conservation equations governing this process can be expressed as follows:

$$\dot{m}_{a5} + \dot{m}_{v5} = \dot{m}_{a6} + \dot{m}_{v6} \tag{17}$$

$$\dot{m}_{a5}h_{a5} + \dot{m}_{v5}h_{v5} = \dot{m}_{a6}h_{a6} + \dot{m}_{v6}h_{v6} + \dot{Q}_{he1} \tag{18}$$

If condensation takes place, the outlet humidity ratio and temperature are iteratively solved using the coupled heat and mass balance equations:

$$\dot{m}_{a5} + \dot{m}_{v5} = \dot{m}_{a6} + \dot{m}_{v6} + \dot{m}_{w14} \tag{19}$$

$$\dot{m}_{a5}h_{a5} + \dot{m}_{v5}h_{v5} = \dot{m}_{a6}h_{a6} + \dot{m}_{v6}h_{v6} + \dot{m}_{w14}h_{w14} + \dot{Q}_{he1} \tag{20}$$

Processes 6 → 7 and 15, and a → b (heat exchange in EHE): Humid air from state 6 passes through the EHE, where it is further cooled, and (if saturation is reached) condensation may occur before the air exits at state 7; condensate is collected at state 15. Simultaneously, the working fluid (denoted by states a → b) absorbs heat in the EHE.

The air may undergo either sensible cooling only or sensible cooling with condensation, depending on whether the outlet state reaches saturation. The outlet temperature is preliminarily estimated from the COP, after which vapor pressure and relative humidity are evaluated. In this process [36]:

$$\dot{Q}_{in} = COP \times \dot{W}_c \tag{21}$$

We check whether condensation occurs during the process by the following equations, calculating p_{v6} as follows:

$$p_{v6} = RH_6 \times \exp\left(\frac{17.27 \times T_6}{T_6 + 237.3}\right), \tag{22}$$

We calculate the dew-point temperature T6′ with mass balance and heat balance:

$$T_{6\prime} = \frac{\dot{Q}_{in}}{1.005\,\dot{m}_{a6} + 1.85\,\dot{m}_{v6}}, \tag{23}$$

and calculate $RH_{6'}$ as follows:

$$RH_{6\prime} = \frac{RH_6 \times \exp\left(\frac{17.27 \times T_6}{T_6 + 237.3}\right)}{\exp\left(\frac{17.27 \times T_{6\prime}}{T_{6\prime} + 237.3}\right)} \tag{24}$$

When the relative humidity at the outlet ($RH_{6'}$) remains below 100%, the process involves only sensible cooling. Otherwise, condensation occurs, and both latent and

sensible heat transfer are considered in the energy balance. Accordingly, the mass and energy conservation equations governing this process can be expressed as follows:

$$\dot{m}_{a6} + \dot{m}_{v6} = \dot{m}_{a7} + \dot{m}_{v7} \tag{25}$$

$$\dot{m}_{a6}h_{a6} + \dot{m}_{v6}h_{v6} = \dot{m}_{a7}h_{a7} + \dot{m}_{v7}h_{v7} + \dot{Q}_{in} \tag{26}$$

If condensation takes place, the outlet humidity ratio and temperature are iteratively solved using the coupled heat and mass balance equations:

$$\dot{m}_{a6} + \dot{m}_{v6} = \dot{m}_{a7} + \dot{m}_{v7} + \dot{m}_{w15} \tag{27}$$

$$\dot{m}_{a6}h_{a6} + \dot{m}_{v6}h_{v6} = \dot{m}_{a7}h_{a7} + \dot{m}_{v7}h_{v7} + \dot{m}_{w15}h_{w15} + \dot{Q}_{in} \tag{28}$$

Processes 7 → 8 and 10 (air splits via valves Val_1 and Val_2): The air stream is split into two separate paths by valves Val_1 and Val_2. This split allows part of the airflow to be recirculated or bypassed, depending on the operational mode, while the remaining portion proceeds along the main circuit. During the splitting process, the total mass of dry air and water vapor is conserved, and no condensation occurs:

$$\dot{m}_{a8} + \dot{m}_{v8} = OP_{val1} \times \left(\dot{m}_{a7} + \dot{m}_{v7}\right) \tag{29}$$

$$\dot{m}_{a10} + \dot{m}_{v10} = OP_{val2} \times \left(\dot{m}_{a7} + \dot{m}_{v7}\right) \tag{30}$$

Process 10 → 11 (passing heat exchanger 2): The air from point 10 flows through the partially opened valve Val_2 into HE2, where it exchanges heat with the surrounding air, resulting in an increase in the air temperature. After this ambient heating process, the air continues to the CHE after mixing with fresh ambient air, if any comes through valve Val_3. To simplify the model, the air temperature exiting HE2 was assumed to fixed at 1 °C below the ambient temperature:

$$T_{11} = T_1 - 1 \tag{31}$$

$$\dot{m}_{a10} + \dot{m}_{v10} = \dot{m}_{a11} + \dot{m}_{v11} \tag{32}$$

$$\dot{m}_{a10}h_{a10} + \dot{m}_{v10}h_{v10} = \dot{m}_{a11}h_{a11} + \dot{m}_{v11}h_{v11} \tag{33}$$

By solving Equations (1)–(33) in the mathematical model described above, the 33 variables, including $\dot{m}_{w14}$ and $\dot{m}_{w15}$, can be determined when key known parameters and information (e.g., T_1, RH_1, $\dot{m}_{a2}$, T_{w12}, OP_{val2}, COP, and W_c) are input.

The mathematical model described above is based on the principles of mass and energy conservation. In addition, the thermodynamic properties of moist air calculated from the model, such as humidity ratio, enthalpy, and temperature, were examined to ensure consistency with actual psychrometric behavior under the specified operating conditions and to confirm that the computed values were physically reasonable across all conditions. Therefore, the model is considered to have been verified, although it has not been experimentally validated yet.

3.3. Performance Evaluation Criteria

To assess the performance of the proposed system, the key evaluation criteria used were as follows:

1. Total water yield $\dot{m}_{cond}$ (kg/s), which reflects the overall production capacity of the system, defined as follows:

$$\dot{m}_{cond} = \dot{m}_{w14} + \dot{m}_{w15} \tag{34}$$

2. The energy rate per unit mass of freshwater produced, ε, which is defined as follows:

$$\varepsilon_c = \frac{\dot{W}_c}{3.6 \times (\dot{m}_{14} + \dot{m}_{15})} \quad (35)$$

If fan power is considered:

$$\varepsilon_{c+f} = \frac{\dot{W}_c + \dot{W}_f}{3.6 \times (\dot{m}_{14} + \dot{m}_{15})} \quad (36)$$

3.4. The Reference Case

To provide a comparison base in subsequent analyses, a reference case was established. The reference case represents the steady-state operation of the proposed system, with inlet air, water, and refrigerant parameters given. The values of the input parameters and the results of the reference case are summarized in Table 1.

Table 1. Input and output parameters for the reference case.

Input of the Model			
Parameter	Description	Unit	Value
T_1	Inlet air temperature	°C	35
RH_1	Inlet air relative humidity	%	40
$\dot{m}_{a2}$	Total air mass flow rate	kg/s	3
RH_5	Assumed air relative humidity at outlet of DEU	%	95
T_{w12}	Inlet water temperature (DEU)	°C	28
$\dot{m}_{w12}$	Inlet water mass flow rate (DEU)	kg/s	1
OP_{val2}	The percentage of valve opening of valve Val_2	%	40
W_c	Compressor power input	kW	3
W_f	Fan power input	kW	1.5
COP	Coefficient of performance of the refrigeration unit	–	4
Results of the Reference Case			
Parameter	Description	Unit	Value
$\dot{m}_{evap}$	Evaporation rate (DEU)	kg/h	25.62
$\dot{m}_{w14}$	Condensation water mass flow rate (HE1)	kg/h	4.54
$\dot{m}_{w15}$	Condensation water mass flow rate (EHE)	kg/h	50.06
$\dot{m}_{cond}$	The total water yield	kg/h	54.60
ε_c	The energy rate per unit mass of freshwater produced (compressor)	kWh/m^3	54.94
ε_{c+f}	The energy rate per unit mass of freshwater produced (compressor and fan)	kWh/m^3	82.41

Table 1 shows a reference case established under steady-state conditions to provide a baseline for subsequent analyses. The inlet air temperature (T_1) and relative humidity (RH_1) were 35 °C and 40%, the DEU inlet water temperature (T_{w12}) and flow rate ($\dot{m}_{w12}$) were 28 °C and 1 kg/s, the total air mass flow rate ($\dot{m}_{a2}$) was 3 kg/s, the valve opening (OP_{val2}) was 40%, and the compressor and fan powers (W_c and W_f) were 3 kW and 1.5 kW, respectively. The DEU outlet relative humidity (RH_5) was assumed to be 95%, and the refrigeration unit COP was 4. The auxiliary heat exchangers (HE1 and HE2) were modeled with predefined outlet air

temperatures. Under these conditions, the system produced a DEU evaporation rate ($\dot{m}_{evap}$) of 25.62 kg/h and condensation water flows of 4.54 kg/h through HE1 ($\dot{m}_{w14}$) and 50.06 kg/h through the evaporator ($\dot{m}_{w15}$), yielding a total water output ($\dot{m}_{cond}$) of 54.60 kg/h. The energy consumption per unit mass of freshwater was 54.94 kWh/m^3 for the compressor only (ε_c) and 82.41 kWh/m^3 including the fan (ε_{c+f}). These results provide a reference point for evaluating system performance under varying conditions.

4. Results of Sensitivity Analysis

In order to evaluate the impacts of some key design and operating parameters on system performance, a sensitivity analysis was carried out. The parameters studied included temperature and humidity of fresh intake air, saline water flow rate, and valve opening ratio, i.e., recycled air ratio, etc.

4.1. Effect of Inlet Air Temperature

The inlet air temperature (T_1) has a moderate influence on the condensation performance of the system, as shown in Figure 2; the highlights are the results of the reference case. When T_1 increased from 15 °C to 45 °C, the total water yield ($\dot{m}_{cond}$) increased from 41.0 kg/h to 66.1 kg/h, while its energy rate per unit mass of freshwater produced (ε_c) decreased from 73.1 kWh/m^3 to 45.4 kWh/m^3. The reason this happened was thought to be that warmer ambient air with the same relative humidity resulted in a higher temperature at the inlet and outlet of the DEU and thus more moisture in the air stream available for condensation later in HE1 and the EHE.

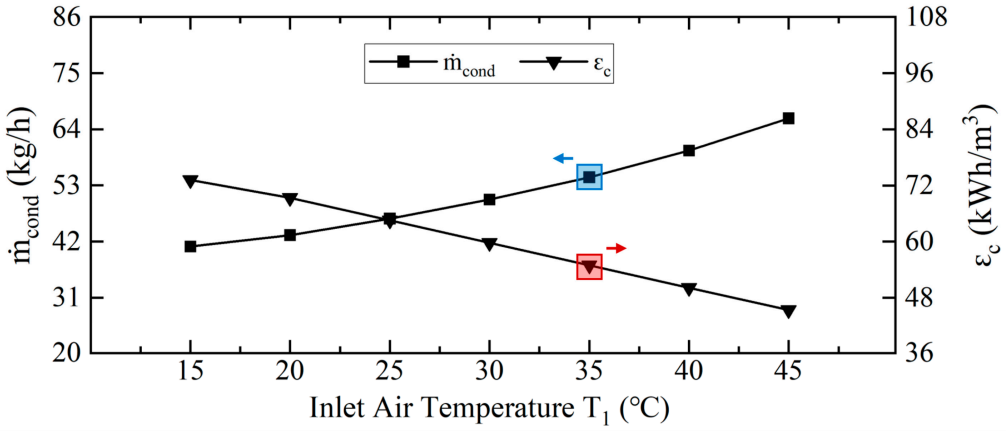

Figure 2. Effect of inlet air temperature on total water yield ($\dot{m}_{cond}$) and the energy rate per unit mass of freshwater produced (ε_c).

4.2. Effect of Inlet Air Relative Humidity

The effect of the relative humidity of the inlet air (RH_1) on the condensation performance is negligible, as shown in Figure 3; the highlights are the results of the reference case. When RH_1 increased from 25% to 55%, the $\dot{m}_{cond}$ increased slightly from 51.5 kg/h to 57.8 kg/h, while ε_c decreased from 87.3 kWh/m^3 to 77.8 kWh/m^3. The result arose from the assumption of the fixed outlet relative humidity of the DEU. Under this assumption, variations in RH_1 had little influence on the condensation process. To address this limitation or remove this assumption, a detailed DEU model would be required, which is beyond the scope of the present study.

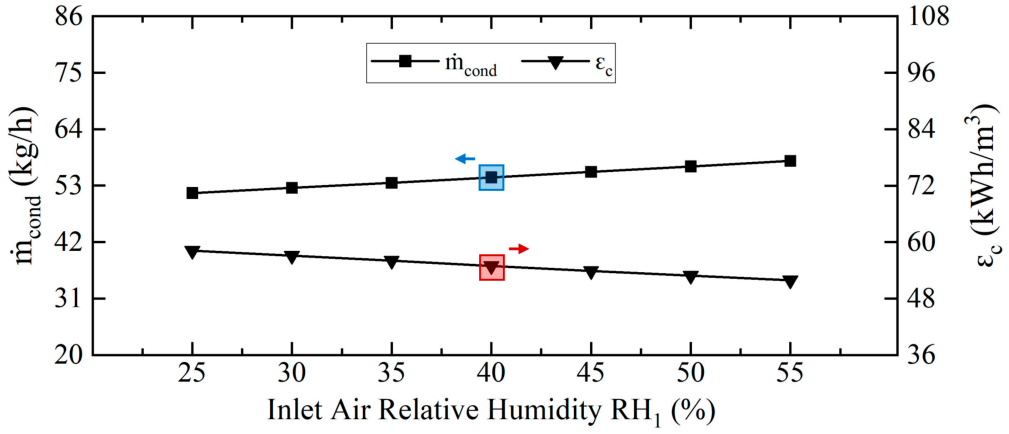

Figure 3. Effect of inlet air relative humidity on total water yield ($\dot{m}_{cond}$) and the energy rate per unit mass of freshwater produced (ε_c).

4.3. Effect of Total Air Mass Flow Rate

The performance of the system is affected by the total mass flow rate of the inlet air ($\dot{m}_{a2}$), as shown in Figure 4; the highlights are the results of the reference case. When the air mass flow rate increased from 1.5 kg/s to 4.5 kg/s, the $\dot{m}_{cond}$ increased from 47.8 kg/h to 57.8 kg/h, while the ε_c continued to decline from 58.2 kWh/m^3 to 51.9 kWh/m^3, indicating that the efficiency of energy utilization had improved. This was because the increase in air flow reduced the temperature drop caused by direct contact with heat and mass transfer in the DEU, thus carrying more water vapor under the relative humidity conditions of the same outlet, increasing the potential amount of water for subsequent condensation. Based on the results, a favorable air flow rate range appeared to be between approximately 3.5 kg/s and 4.5 kg/s, where a relatively high condensation rate was maintained alongside a lower specific energy consumption.

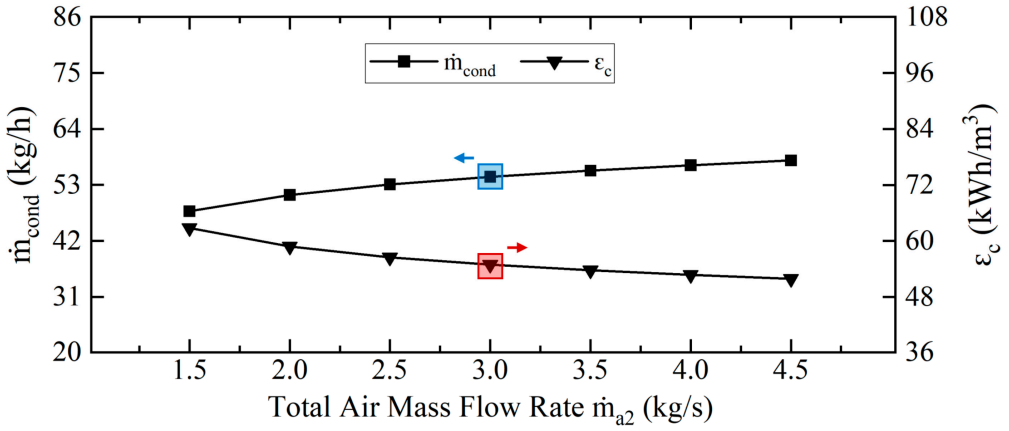

Figure 4. Effect of total air mass flow rate on total water yield ($\dot{m}_{cond}$) and the energy rate per unit mass of freshwater produced (ε_c).

4.4. Effect of Inlet Water Temperature

The effect of inlet water temperature (T_{w12}) on the condensation performance of the system is shown in Figure 5; the highlights are the results of the reference case. As T_{w12} rose from 12 °C to 36 °C, the $\dot{m}_{cond}$ increased significantly from 35.3 kg/h to 65.5 kg/h, while the ε_c decreased from 85.0 kWh/m^3 to 45.8 kWh/m^3. The higher inlet water temperature improved the temperature of the cooling surface, enhanced the heat and mass transfer process between air and water, and reduced the temperature drop in the air in the DEU, so that the air could carry more water vapor under the same relative humidity, making

it more easily able to precipitate condensate in the subsequent condensation stage. The results show that under the condition of maintaining a moderately high inlet water temperature, the water production capacity and overall energy efficiency of the system can be significantly improved.

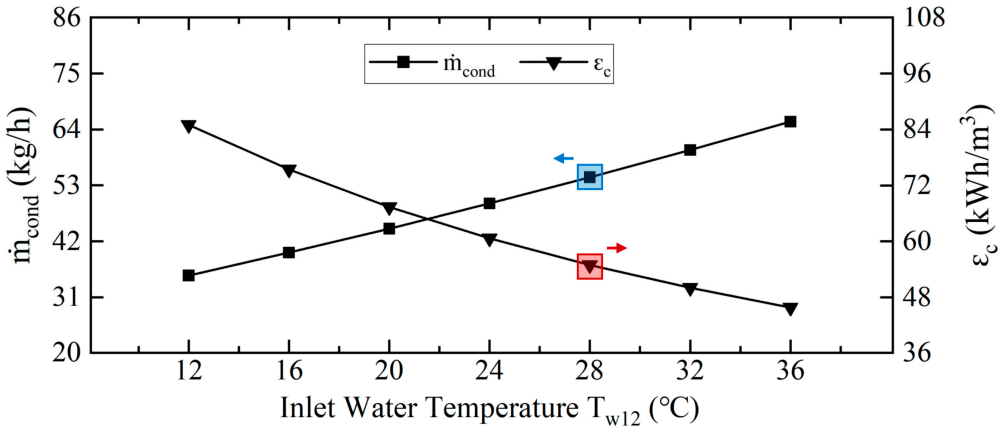

Figure 5. Effect of inlet water temperature on total water yield ($\dot{m}_{cond}$) and the energy rate per unit mass of freshwater produced (ε_c).

4.5. Effect of Inlet Water Mass Flow Rate

The effect of the inlet water mass flow rate ($\dot{m}_{w12}$) is shown in Figure 6; the highlights are the results of the reference case. As the water flow rate increased from 0.25 kg/s to 1.75 kg/s, the $\dot{m}_{cond}$ and ε_c only changed slightly, indicating that the system performance is not sensitive to changes in water flow within this range. This slight increase in water production was mainly due to the fact that, with the increase in water flow, the temperature drop per unit mass of water caused by evaporation-related latent heat was partially offset, and the temperature drop on the water side was slightly reduced, so the surface temperature of the water was relatively higher, thus carrying more potentially condensable water vapor.

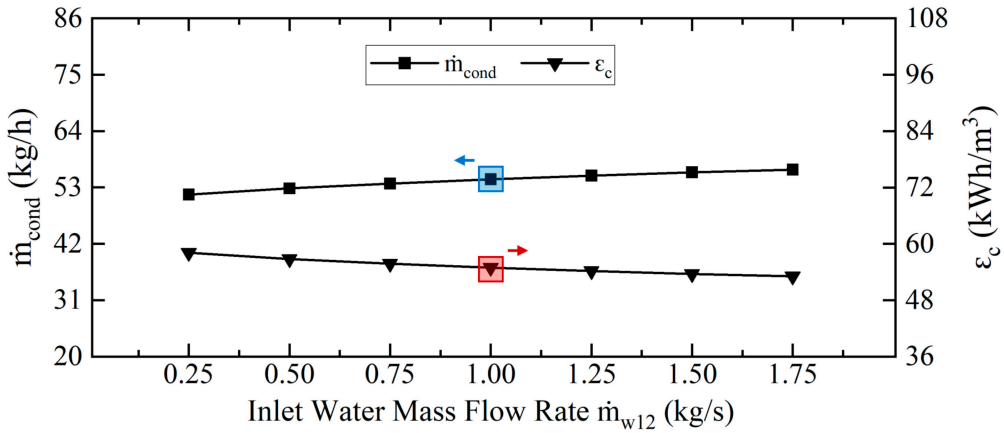

Figure 6. Effect of inlet water mass flow rate on total water yield ($\dot{m}_{cond}$) and the energy rate per unit mass of freshwater produced (ε_c).

In addition, this phenomenon is also related to the model hypothesis that the relative humidity of the outlet air in the DEU remains constant. Under this hypothesis, the additional water flow rate will not significantly change the saturation state of the air or the thermal balance of the system as a whole. Therefore, when the water mass flow exceeds a certain level, its effect on improving the condensation water output or system energy efficiency should be limited.

4.6. Effect of Compressor Power Input

The compressor power input (W_c) directly determines the refrigeration capacity of the system, as shown in Figure 7; the highlights are the results of the reference case. With the increase in W_c from 1.5 kW to 4.5 kW, the $\dot{m}_{cond}$ increased markedly from 30.7 kg/h to 76.5 kg/h. The reason for this significant increase is that in the NeWater system, the VRU contributes in two ways: by providing evaporation cooling (Q_{in}) to condense the moisture in the air stream and by releasing condensing heat (Q_{out}) to pre-heat air entering the DEU. When W_c increased with fixed *COP*, both Q_{in} and Q_{out} increased.

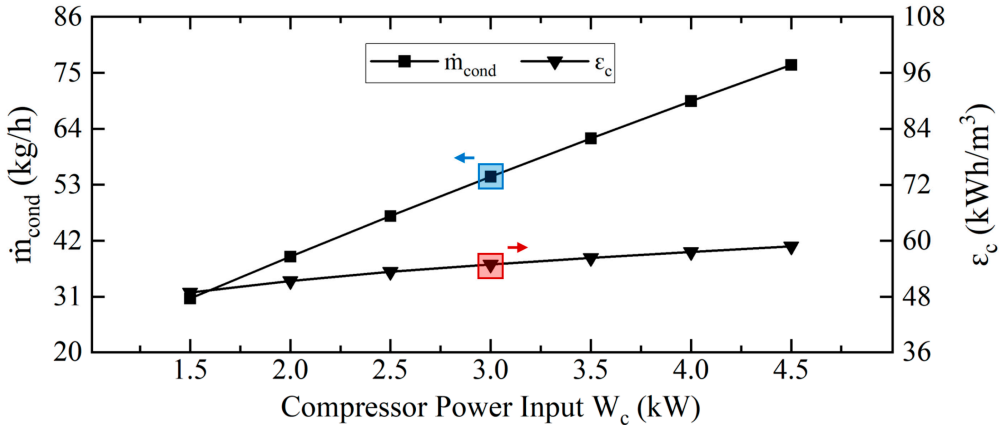

Figure 7. Effect of compressor power input on total water yield ($\dot{m}_{cond}$) and the energy rate per unit mass of freshwater produced (ε_c).

However, the increase in condensation was accompanied by an increase in energy consumption. The ε_c continued to rise with the increase in W_c, increasing from 48.9 kWh/m^3 to 58.8 kWh/m^3, indicating that the marginal return of the unit of additional water output was decreasing as the electricity input increased. Under the high compressor power input, most of the extra energy was used for sensible cooling, not condensation through latent heat. Therefore, when the compressor power exceeded the moderate level, although the water output continued to increase, the energy efficiency of the system showed a decreasing trend.

4.7. Effect of Coefficient of Performance

The coefficient of performance (*COP*) of the VRU represents its efficiency and significantly influences the behavior of the NeWater system, as shown in Figure 8; the highlights are the results of the reference case. As the COP increases from 2.5 to 5.5, the condensation rate ($\dot{m}_{cond}$) rises linearly from 37.0 to 71.0 kg/h. In contrast, the specific energy consumption (ε_c) exhibits a different trend: it first decreases sharply and then stabilizes, dropping from 81.1 to 42.3 kWh/m^3. This is because, with a fixed W_c, an increase in *COP* leads to higher Q_{in} and Q_{out}, enhancing both the evaporation and condensation processes within the system. This indicates the importance of VRU design, especially its COP, in determining system performance.

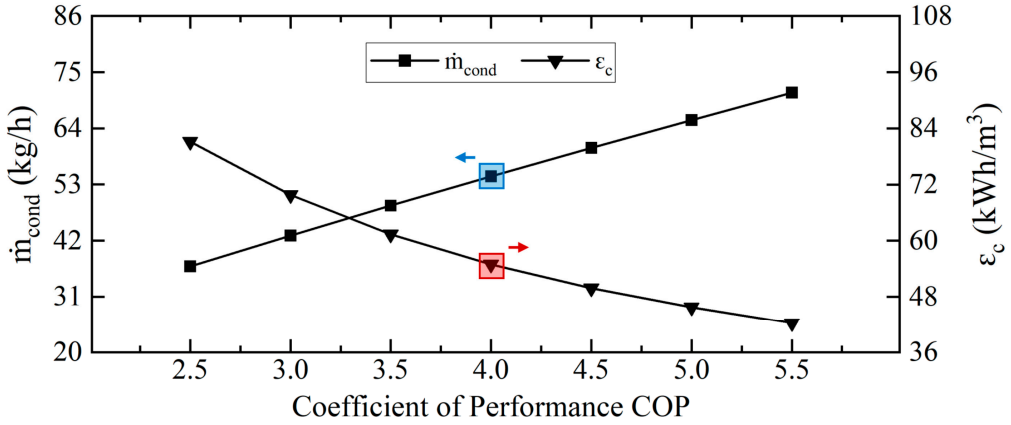

Figure 8. Effect of coefficient of performance on total water yield ($\dot{m}_{cond}$) and the energy rate per unit mass of freshwater produced (ε_c).

4.8. Effect of Percentage of Recirculated Air Loop

The opening of valve 2 (OP_{val2}), which governs the air circulation ratio, affects the humidity and enthalpy of air in the system. As shown in Figure 9, the highlights are results of the reference case, with the circulation ratio increasing from 0% (fully open) to 100% (fully closed); the condensation rate ($\dot{m}_{cond}$) decreases from 62.3 to 43.8 kg/h. Conversely, the specific energy consumption (ε_c) shows an opposite trend, increasing from 48.2 to 68.5 kWh/m^3. In the open system, the continuous inflow of fresh ambient air provides new moisture for condensation. In contrast, at a higher circulation ratio, the temperature of the reflux air is lower, and the amount of water vapor carried by the air coming out of the DEU is reduced, which reduces the condensation potential, thus limiting the water output. This effect is further influenced by the assumption of a fixed outlet relative humidity at the DEU, which constrains the variation in air moisture content.

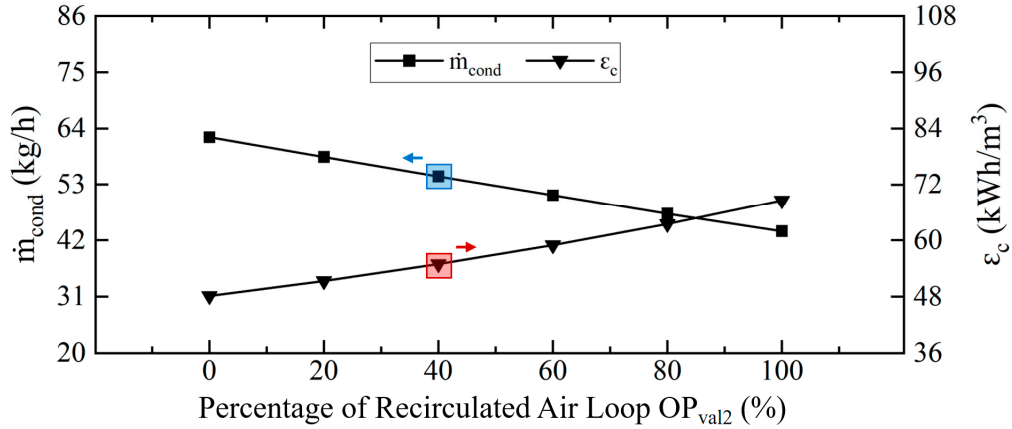

Figure 9. Effect of percentage of recirculated air loop on total water yield ($\dot{m}_{cond}$) and the energy rate per unit mass of freshwater produced (ε_c). OP values of 100% mean closed loop (CL) operation, while OP values of 0% mean fully open loop (OL) operation.

4.9. Effect of Air Relative Humidity at Outlet of DEU

The relative humidity of the outlet air of the DEU (i.e., the cooling tower), RH_5, indicates the humidity saturation level, which depends on the design, structure, and operation of the DEU. In this study, the DEU was treated as a black box, and its outlet relative humidity was assumed. As shown in Figure 10, the highlights are results of the reference case, in which RH_5 increases from 85% to 100%, the $\dot{m}_{cond}$ increases from 31.6 kg/h to 64.4 kg/h, and the ε_c decreases rapidly at first and then levels off from 94.9 kWh/m^3 to 46.6 kWh/m^3, indicating that the system is close to its maximum condensation potential.

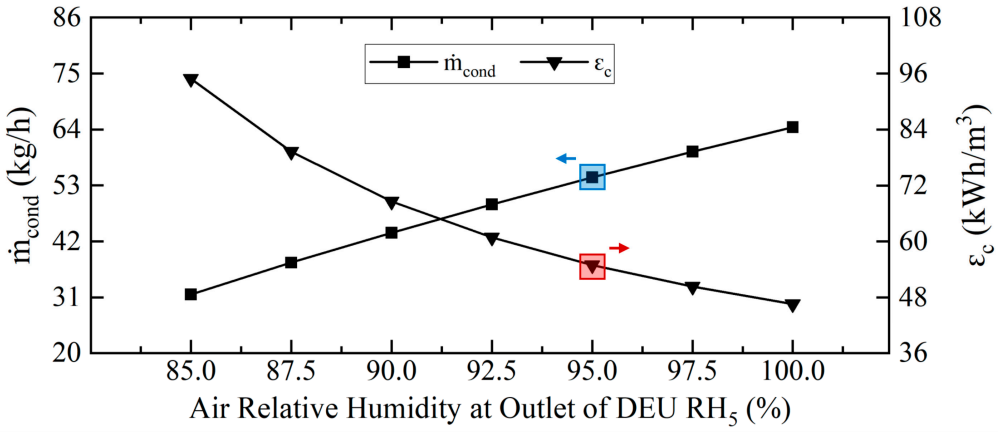

Figure 10. Effect of air relative humidity at outlet of the DEU on total water yield ($\dot{m}_{cond}$) and the energy rate per unit mass of freshwater produced (ε_c).

These results highlight the importance of DEU design: in order to maximize system efficiency, the air–water interface must provide a large contact area, optimal water droplet atomization, and sufficient residence time for full saturation. Appropriately enhancing these parameters can significantly improve water production and energy utilization in future system optimization.

5. Conclusions

This paper proposed a NeWater system to achieve freshwater production in an environment where it is difficult to apply traditional seawater desalination technologies. The system can flexibly switch the operation mode to adapt to different ambient temperature, humidity, and water source conditions. The system performance is simulated by a mathematical model developed based on thermodynamic principles. The impacts of several key design and operation parameters on the system performance were studied. When compared with the performance of standalone desalination [15] or atmospheric water harvesting systems [27], the integrated NeWater system proposed in this work demonstrates a competitive advantage in achieving simultaneous water production from different sources under a wider range of conditions, although its current unit water production energy consumption is higher than that of currently mature technologies. Based on the results of the sensitivity study, the following conclusions can be drawn:

1. The increase in the ambient air temperature and the relative humidity of the inlet air can significantly improve the performance of the system (including increasing the total water yield and reducing the energy rate per unit mass of freshwater produced), with the effect of air temperature being the most significant, leading to an increase in the total water yield by up to 1.6 times and a reduction in the energy rate by up to 38%.
2. Increasing the total air mass circulated through the system can improve the performance of the system, with water yield increasing by up to 21% and energy rate decreasing by up to 38%.
3. The increase in the inlet water temperature can enhance heat transfer, reduce the air temperature drop, and increase the moisture content of the air inside the DEU, resulting in the water yield increasing by up to 1.8 times and the energy rate decreasing by up to 46%, while the increase in the inlet water flow rate has less of an impact on the performance of the system and can only slightly increase the water output.
4. Increasing the compressor power or system COP can effectively increase the total water yield. An improvement in COP can enhance the efficiency of the VRU and

enhance the condensation potential, with water yield increasing by up to 1.9 times and energy consumption per unit of freshwater reduced by up to 48%.

5. An improvement in DEU performance, i.e., an increase in the relative humidity at the outlet of the DEU, would improve the system performance effectively. In other words, the design, the structure, and the operation of the DEU are key to system performance, with water yield increasing twofold and energy rate decreasing by up to 51%.

In summary, the results show that the operating parameters—such as the recycling ratio, the mass flow rates of air and water, and the ambient conditions (e.g., the temperatures of air and water)—and the design parameters (e.g., compressor power and COP) jointly affect the performance of the system.

Further improving the simulation model by eliminating the assumption about the RH_5 will be the research focus of the next phase, so that optimization of the key design and operation parameters and the system structure can be carried out, which are beyond the scope of the present paper. A direct comparison with experimental data for a comprehensive validation is an essential next step and is planned as immediate future work. The proposed system demonstrates potential for practical applications in off-grid and water-scarce regions where conventional RO and thermal-based technologies are unavailable.

Author Contributions: Conceptualization, E.H. and J.W.; methodology, E.H. and Y.H.; software, Y.H.; formal analysis, Y.H.; investigation, Y.H.; writing—original draft preparation, Y.H.; writing—review and editing, E.H. and J.W.; supervision, E.H. and J.W. All authors have read and agreed to the published version of the manuscript.

Funding: This research received no external funding.

Data Availability Statement: The original contributions presented in this study are included in the article. Further inquiries can be directed to the corresponding author.

Acknowledgments: The authors would like to acknowledge the School of Mechanical Engineering at Adelaide University for their support. The computations in this work were performed using the Phoenix HPC service at Adelaide University.

Conflicts of Interest: The authors declare no conflicts of interest.

Abbreviations

Nomenclature

A	Drenching water area (m^2)
CHE	Condenser heat exchanger
CL	Closed loop
COP	Coefficient of performance
DEU	Direct evaporation unit
EHE	Evaporator heat exchanger
h	Specific enthalpy (kJ/kg)
h_m	Convective mass-transfer coefficient (kg/(m^2·s))
HE1	Cooling recovery heat exchanger
HE2	Ambient air heat exchanger
L	Latent heat of vaporization (kJ/kg)
$\dot{m}$	Mass flow rate of fluid (kg/s)
OL	Open loop
OP	Valve opening, (%)

P	Pressure (Pa)
Q	Heat (kW)
RH	Air relative humidity (%)
T	Temperature, (°C)
VRU	Vapor compression refrigeration unit
Val	Valve
W	Power input (kW)
Special characters	
ω	Absolute humidity of the air (kg/kg)
ε	Efficiency (kWh/m^3)
Subscripts	
a	Air
c	Compressor
cond	Condensate water
evap	Evaporation
f	Fan
in	Inlet
out	Outlet
v	Vapor
w	Water

References

1. Martínez-Alvarez, V.; Martin-Gorriz, B.; Soto-García, M. Seawater desalination for crop irrigation—A review of current experiences and revealed key issues. *Desalination* **2016**, *381*, 58–70. [CrossRef]
2. Zhang, G.; Wang, X. Seawater Desalination System Driven by Sustainable Energy: A Comprehensive Review. *Energies* **2024**, *17*, 5706. [CrossRef]
3. Hu, J.; Sun, Y.; Liu, Z.; Zhu, B.; Zhang, L.; Xu, N.; Zhu, M.; Zhu, J.; Chen, Z. Photothermal fabrics for solar-driven seawater desalination. *Prog. Mater. Sci.* **2025**, *150*, 101407. [CrossRef]
4. Simmons, J.W., II; Van de Ven, J.D. A Comparison of Power Take-Off Architectures for Wave-Powered Reverse Osmosis Desalination of Seawater with Co-Production of Electricity. *Energies* **2023**, *16*, 7381. [CrossRef]
5. Adityawarman, D.; Lugito, G.; Kawi, S.; Wenten, I.G.; Khoiruddin, K. Advancements and future trends in nanostructured membrane technologies for seawater desalination. *Desalination* **2025**, *597*, 118390. [CrossRef]
6. Bacha, H.B.; Abdullah, A.S.; Aljaghtham, M.; Salama, R.S.; Abdelgaied, M.; Kabeel, A.E. Thermo-Economic Assessment of Photovoltaic/Thermal Pan-Els-Powered Reverse Osmosis Desalination Unit Combined with Preheating Using Geothermal Energy. *Energies* **2023**, *16*, 3408. [CrossRef]
7. Barron, O.; Ali, R.; Hodgson, G.; Smith, D.; Qureshi, E.; McFarlane, D.; Campos, E.; Zarzo, D. Feasibility assessment of desalination application in Australian traditional agriculture. *Desalination* **2015**, *364*, 33–45. [CrossRef]
8. Al-Obaidi, M.; Alsarayreh, A.A.; Rashid, F.L.; Sowgath, M.T.; Alsadaie, S.; Ruiz-García, A.; Khayet, M.; Ghaffour, N.; Mujtaba, I.M. Hybrid membrane and thermal seawater desalination processes powered by fossil fuels: A comprehensive review, future challenges and prospects. *Desalination* **2024**, *583*, 117694. [CrossRef]
9. Zhou, X.; Lu, H.; Zhao, F.; Yu, G. Atmospheric Water Harvesting: A Review of Material and Structural Designs. *ACS Mater. Lett.* **2020**, *2*, 671–684. [CrossRef]
10. Tan, B.; Liu, Y.; Ren, H.; Gong, Z.; Li, X.; Li, W.; Guo, L.; Chen, R.; Wei, J.; Dai, Q.; et al. N, S-carbon quantum dots as inhibitor in pickling process of heat exchangers for enhanced performance in multi-stage flash seawater desalination. *Desalination* **2024**, *589*, 117969. [CrossRef]
11. Su, Y.; Gu, R.; Li, Y.; Wu, W.; Yu, Z.; Cheng, S. Seawater interfacial evaporation in composite gel enables photovoltaic cooling, simultaneous seawater desalination, and enhanced uranium extraction. *Adv. Funct. Mater.* **2025**, 2420651. [CrossRef]
12. Shahzad, M.W.; Burhan, M.; Ybyraiymkul, D.; Ng, K.C. Desalination Processes' Efficiency and Future Roadmap. *Entropy* **2019**, *21*, 84. [CrossRef] [PubMed]
13. Shenvi, S.S.; Isloor, A.M.; Ismail, A.F. A review on RO membrane technology: Developments and challenges. *Desalination* **2015**, *368*, 10–26. [CrossRef]
14. Chen, Z.; Su, C.; Zhan, H.; Chen, L.; Wang, W.; Zhang, H.; Chen, X.; Sun, C.; Kong, Y.; Yang, L.; et al. Thermodynamic and economic analyses of nuclear power plant integrating with seawater desalination and hydrogen production for peak shaving. *Int. J. Hydrogen Energy* **2025**, *82*, 1372–1388. [CrossRef]

15. Ma, J.; Sun, X.; Wang, L.; An, M.; Kim, M.; Yamauchi, Y.; Khaorapapong, N.; Yuan, Z. Bio-inspired 3D architectured aerogel evaporator for highly efficient solar seawater desalination. *Nano Energy* **2025**, *137*, 110781. [CrossRef]
16. Shin, Y.; Koo, J.; Lee, S. System Dynamics Modeling of Scale Formation in Membrane Distillation Systems for Seawater and RO Brine Treatment. *Membranes* **2024**, *14*, 252. [CrossRef]
17. Zhou, Y.; Khan, B.; Gu, H.; Christofides, P.D.; Cohen, Y. Modeling UF fouling and backwash in seawater RO feedwater treatment using neural networks with evolutionary algorithm and Bayesian binary classification. *Desalination* **2021**, *513*, 115129. [CrossRef]
18. Tashtoush, B.; Alshoubaki, A. Atmospheric water harvesting: A review of techniques, performance, renewable energy solutions, and feasibility. *Energy* **2023**, *280*, 128186. [CrossRef]
19. Zhang, B.; Wong, P.W.; Guo, J.; Zhou, Y.; Wang, Y.; Sun, J.; Jiang, M.; Wang, Z.; An, A.K. Transforming Ti3C2Tx MXene's intrinsic hydrophilicity into superhydrophobicity for efficient photothermal membrane desalination. *Nat. Commun.* **2022**, *13*, 3315. [CrossRef]
20. Lu, D.; Zhou, Z.; Wang, Z.; Ho, D.T.; Sheng, G.; Chen, L.; Zhao, Y.; Li, X.; Cao, L.; Schwingenschlögl, U.; et al. An Ultrahigh-Flux Nanoporous Graphene Membrane for Sustainable Seawater Desalination using Low-Grade Heat. *Adv. Mater.* **2022**, *34*, 2109718. [CrossRef]
21. Gong, D.; Wen, B.; Wang, L.; Zhang, H.; Chen, H.; Fan, J.; Li, Z.; Guo, L.; Zhu, Z.; Liu, X.; et al. Alkadiyne–Pyrene Conjugated Frameworks with Surface Exclusion Effect for Ultrafast Seawater Desalination. *J. Am. Chem. Soc.* **2024**, *146*, 3075–3085. [CrossRef] [PubMed]
22. Su, Q.; Zhang, J.; Zhang, L.-Z. Fouling resistance improvement with a new superhydrophobic electrospun PVDF membrane for seawater desalination. *Desalination* **2020**, *476*, 114246. [CrossRef]
23. Tu, R.; Hwang, Y. Reviews of atmospheric water harvesting technologies. *Energy* **2020**, *201*, 117630. [CrossRef]
24. Wang, J.; Yang, Z.; Li, Z.; Fu, H.; Chen, J. Comprehensive review on atmospheric water harvesting technologies. *J. Water Process Eng.* **2025**, *69*, 106836. [CrossRef]
25. Bai, S.; Chao, L.C.; Pan, A.; Ho, T.C.; Lin, K.; Tso, C.Y. Study of the relative humidity effects on the water condensation performance of adsorption-based atmospheric water harvesting using passive radiative condensers. *Appl. Therm. Eng.* **2024**, *244*, 122702. [CrossRef]
26. Ozkan, O.; Wikramanayake, E.D.; Bahadur, V. Modeling humid air condensation in waste natural gas-powered atmospheric water harvesting systems. *Appl. Therm. Eng.* **2017**, *118*, 224–232. [CrossRef]
27. Deng, F.; Chen, Z.; Wang, C.; Xiang, C.; Poredoš, P.; Wang, R. Hygroscopic Porous Polymer for Sorption-Based Atmospheric Water Harvesting. *Adv. Sci.* **2022**, *9*, 2204724. [CrossRef]
28. Yang, K.; Pan, T.; Lei, Q.; Dong, X.; Cheng, Q.; Han, Y. A Roadmap to Sorption-Based Atmospheric Water Harvesting: From Molecular Sorption Mechanism to Sorbent Design and System Optimization. *Environ. Sci. Technol.* **2021**, *55*, 6542–6560. [CrossRef] [PubMed]
29. Entezari, A.; Esan, O.C.; Yan, X.; Wang, R.; An, L. Sorption-Based Atmospheric Water Harvesting: Materials, Components, Systems, and Applications. *Adv. Mater.* **2023**, *35*, 2210957. [CrossRef]
30. Ying, W.; Li, C.; Yang, L.; Hua, L.; Zhang, H.; Wang, R.; Wang, J. Global potential of continuous sorption-based atmospheric water harvesting Global potential of continuous sorption-based atmospheric water harvesting. *iScience* **2025**, *28*, 112160. [CrossRef]
31. Wang, J.; Huo, E. Opportunities and challenges of seawater desalination technology. *Front. Energy Res.* **2022**, *10*, 960537. [CrossRef]
32. Ayaz, M.; Namazi, M.A.; ud Din, M.A.; Ershath, M.M.; Mansour, A. Sustainable seawater desalination: Current status, environmental implications and future expectations. *Desalination* **2022**, *540*, 116022. [CrossRef]
33. Lu, H.; Shi, W.; Guo, Y.; Guan, W.; Lei, C.; Yu, G. Materials engineering for atmospheric water harvesting: Progress and perspectives. *Adv. Mater.* **2022**, *34*, 2110079. [CrossRef]
34. Wang, J.; Hua, L.; Li, C.; Wang, R. Atmospheric water harvesting: Critical metrics and challenges. *Energy Environ. Sci.* **2022**, *15*, 4867–4871. [CrossRef]
35. Moran, M.J. *Fundamentals of Engineering Thermodynamics*, 8th ed.; Wiley: Hoboken, NJ, USA, 2014.
36. Trott, A.R.; Welch, T.; Hundy, G.F. *Refrigeration and Air-Conditioning*, 4th ed.; Butterworth Heinemann: Oxford, UK, 2008.
37. Katinas, C.; d'Entremont, B.; Ray, W.; Willis, M.; Reichardt, T. Assessing parallel path cooling tower performance via artificial neural networks. *Ann. Nucl. Energy* **2023**, *192*, 109993. [CrossRef]
38. Navarro, P.; Serrano, J.M.; Roca, L.; Palenzuela, P.; Lucas, M.; Ruiz, J. A comparative study on predicting wet cooling tower performance in combined cooling systems for heat rejection in CSP plants. *Appl. Therm. Eng.* **2024**, *253*, 123718. [CrossRef]